X-ray photoelectron diffraction study of relaxation and rumpling of ferroelectric domains in $BaTiO_3(001)$

Alexandre Pancotti,[1,2,3] Jiale Wang,[1] Peixuan Chen,[4] Ludovic Tortech,[5,6] Cristian-Mihail Teodorescu,[7] Emmanouil Frantzeskakis,[8] and Nicholas Barrett[1,*]

[1]*IRAMIS/SPCSI/LENSIS, F-91191 Gif-sur-Yvette, France*

[2]*Departamento de Fisica Aplicada, Universidade Estadual de Campinas, Rua Sergio Buarque de Holanda, 777, Ciudade Universitária Zeferino Vaz, SP, 13083-859, Brazil*

[3]*Universidade Federal de Goiás, CAJ, Laboratório de Ciências Exatas. Rodovia BR 364, km 192, Caíxa Postal 03 75801-615 Jataí - GO, Brazil*

[4]*Institute of Semiconductor and Solid State Physics, Johannes Kepler University Linz, Altenbergerstr. 69, A-4040 Linz, Austria*

[5]*CEA, IRAMIS, SPCSI, LEPO, F- 91191 Gif sur Yvette cedex, France*

[6]*UPMC, IPCM, UMR CNRS 7201, 4 place Jussieu, 75005 Paris, France*

[7]*National Institute of Materials Physics, P.O. Box MG-7, 105 bis Atomistilor St. 077125 Magurele-Ilfov, Romania*

[8]*Synchrotron SOLEIL, L'Orme des Merisiers, Saint Aubin-BP 48, 91192 Gif sur Yvette Cedex, France*

(Received 30 March 2013; revised manuscript received 7 May 2013; published 28 May 2013)

The surface of a ferroelectric $BaTiO_3(001)$ single crystal was studied using synchrotron radiation induced x-ray photoelectron diffraction (XPD), x-ray photoelectron spectroscopy (XPS), atomic force microscopy (AFM), and low-energy electron diffraction (LEED). AFM, XPS, and LEED show that the surface is BaO terminated with a (1×1) reconstruction. The Ba $4d$, Ti $2p$, and O $1s$ XPD results were compared with multiple scattering simulations for out-of- (P^+,P^-) and in-plane (P^{in}) polarizations using a genetic algorithm to determine atomic rumpling and interlayer relaxation. Linear combinations of the XPD simulations of the surface structure of each polarization state allow determination of the domain ordering. The best agreement with experiment is found for 55% P^+, 38% P^-, and 7% P^{in}. The rumpling is smaller at the surface than in the bulk, suggesting that both domain ordering and surface structural changes contribute to screening of the polarization.

DOI: 10.1103/PhysRevB.87.184116 PACS number(s): 73.22.Pr, 61.48.Gh, 79.60.−i

I. INTRODUCTION

The surface of a ferroelectric (FE) may show a net fixed polarization charge which is intrinsically unstable due to the well-known polar catastrophe.[1] The presence of unscreened surface charge creates an internal electric field, the depolarizing field, which can partially or wholly cancel the polarization inside the material. Thus, the electrical boundary conditions can destabilize the ferroelectric state. The surface polarization charge can be screened by a variety of mechanisms including adsorbate species,[2,3] intrinsic defects,[4] free charge carriers, surface and near-surface structural changes (rumpling, relaxation, and reconstruction), and domain ordering.[5] The latter reduces the energy of the system by screening the depolarizing field through ordering of the FE domains with antiparallel dipole moments.[6] The depolarizing field in one domain is screened by the electric fields of adjacent domains. However, such screening is usually imperfect. In the absence of significant adsorbates or free charge carriers, intrinsic defects and structural changes may combine with domain ordering to minimize the energy of the system and strongly influence its FE properties.[7] Understanding how the microscopic screening mechanisms may combine with domain ordering is therefore important in predicting and controlling ferroelectric stability.

Here, we investigate the surface relaxation and atomic rumpling of an archetypal ferroelectric, single-crystal $BaTiO_3$ (BTO). BTO is a perovskite oxide consisting of alternating BaO and TiO_2 atomic layers along the [001] direction. Above the Curie temperature ($\sim$120 °C), it has a centrosymmetric paraelectric cubic structure with five atoms per unit cell ($Pm3m$). At lower temperatures, the crystal has three successive FE (noncentrosymmetric) phases. The room-temperature phase is tetragonal with lattice parameters $a = 3.996$ Å and $c = 4.036$ Å. In the tetragonal phase, there are two FE distortions along the c axis, parallel and antiparallel to [001] identified as P^+ and P^- in Fig. 1. The polarization may also be along one of the four equivalent a-axis directions, identified as P^{in}. When considering the (001) surface, the four in-plane polarizations are equivalent, whereas symmetry breaking at the surface distinguishes P^+ and P^-.

The ideal (001) surface termination can either be BaO or TiO_2. Kolpak *et al.*[8] investigated the surface phase diagram of BTO as a function of sample preparation and report that after UHV annealing at 700 °C the (1×1) surface is mainly BaO terminated. Given the room-temperature tetragonal structure, the FE polarization may be out of plane $P^{\pm}$, with dipole moments pointing exclusively up from or down to the surface along the c axis or in plane along either the a or b axes. The particular domain ordering is dependent on sample history and can include both 180° (antiparallel) and 90° (top to tail) domain walls.[5,9] Surface rumpling and interplanar relaxation must also be considered for each type of domain. Surface structural modifications have been the subject of theoretical studies.[10–12] Following Meyer and Vanderbilt,[12] relaxation is given by the average atomic displacement $\beta = [\delta_z(M) + \delta_z(O)]/2$, where $\delta_z(M)$ and $\delta_z(O)$ are the displacements of the Ba or Ti ions and the oxygen ions, respectively, from the bulk positions. The change in the interlayer spacing Δd_{ij} is the difference in the average atomic displacements for two adjacent layers β_i and β_j. The intralayer corrugation or rumpling is defined as $\eta = [\delta_z(M) - \delta_z(O)]/2$. The surface plane is indexed $i = 1$.

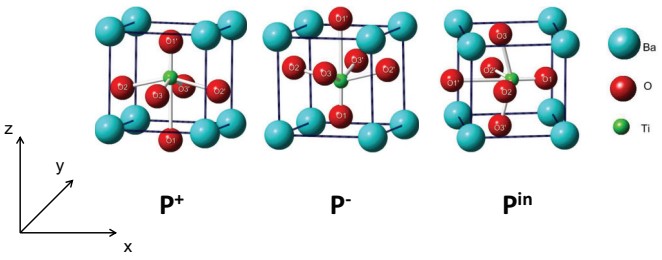

FIG. 1. (Color online) Schematic of FE distortion in the BTO unit cell for P^+, P^-, and P^{in} (in this case, P_x) polarizations. Displacements are exaggerated for clarity.

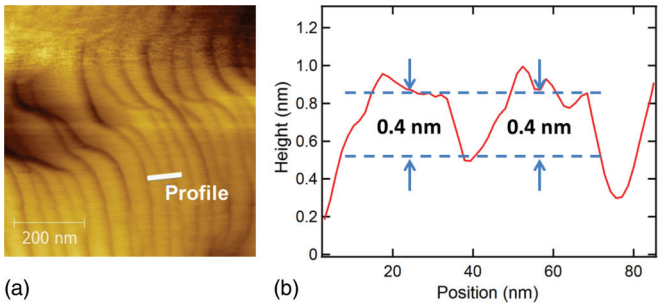

FIG. 2. (Color online) (a) AFM topography image of BTO(001) surface after annealing at 900 °C with a flow rate of 5l/min for 3 h in O_2, (b) line profiles showing the appearance of unit-cell steps after annealing in oxygen.

Experimentally probing such surfaces requires a structural tool sensitive to local atomic positions and to surface chemistry. X-ray photoelectron diffraction (XPD) combines such chemical sensitivity with quantitative information on the local atomic structure around each emitting atom.[13] In comparison to another well-established surface-structure technique, low-energy electron diffraction (LEED), XPD is element specific. It can provide information about the atomic distortions in and below the surface layer around each chemical species. It is therefore an ideal tool to probe such elemental specific local distortions at the surface of FE materials. However, few XPD studies of FE oxides have appeared in the literature. Schneider *et al.* performed an early study of perovskite oxides using forward focusing.[14] Berlich *et al.* have investigated the surface chemistry of paraelectric BTO,[15] while Despont *et al.* have published high-resolution XPD and x-ray diffraction (XRD) studies of the FE distortion in a $PbTiO_3$ thin film.[16,17] By using synchrotron radiation, the kinetic energy of the photoelectrons can be tuned so as to favor the more bulk-sensitive, forward scattering, or the more surface-sensitive multiple scattering regimes.[18] One experimental study of the atomic rumpling and relaxation for P^+ polarization in a thin film has been published using LEED.[19]

The aim of this work was to study the relaxation, rumpling, and domain ordering at the surface of the model FE BTO(001). The paper is organized as follows. The experimental and theoretical methods are presented. Atomic force microscopy (AFM), high-resolution x-ray photoelectron spectroscopy (XPS), and LEED results provide information on the morphology, chemistry, and structure of the surface. Then, the Ba $4d$, Ti $2p$, and O $1s$ XPD experimental results and multiple scattering simulations are presented and discussed, leading to a quantitative description of both domain ordering and surface atomic rumpling and relaxation.

II. EXPERIMENTAL AND THEORETICAL METHODS

A. Experiment

The sample was a 7.5×7.5 mm^2 BTO single crystal furnished by MaTecK GmbH. Figure 2 shows an AFM topography image of the BTO(001) surface after annealing at 900 °C in O_2 with a flow rate of 5l/min for 3 h. Wide, flat terraces with mainly 0.4-nm step heights are observed, indicating a single surface termination [Fig. 2(b)].

The XPD experiments were carried out at the Antares beamline, Synchrotron Soleil (Saint Aubin). An electrostatic hemispherical analyzer (Scienta 4000) was used allowing simultaneous detection of emitted electrons over a wide angular range without tilting of the sample. All the data were normalized by the background to each spectrum in the XPD pattern. The 700-eV photon energy was chosen to increase surface sensitivity and to ensure that the XPD data included multiple scattering. The sample was ozone cleaned *ex situ* for 1 h before introduction into the vacuum system. It was then annealed *in situ* in O_2 (2×10^{-4} Pa) for several hours to remove residual organic contaminations on the surface. The base pressure of the system was better than 3×10^{-8} Pa. Stoichiometric BTO has a ~3.2-eV band gap rendering it difficult for x-ray photoelectron spectroscopy experiments due to charging. To overcome this problem, the sample was annealed in UHV at 740 °C for 1 h. This procedure created oxygen vacancies,[20,21] increasing the sample conductivity. The inset of Fig. 3(a) shows a typical (1×1) LEED pattern for BTO(001) single crystal after annealing. The LEED has fourfold symmetry, therefore the experimental azimuthal angular range guarantees that all diffracting structures were measured and that symmetrization of the data set could be used to plot the XPD patterns over 2π. The LEED spots could be sharper, but as the O and C $1s$ XPS shows, there is some residual surface contamination. The low anisotropy and low statistics in the C $1s$ XPD [Fig. 4(d)] suggest, however, that the surface contamination is disordered. Thus, although some long-range disorder may be present, it should not affect the essential conclusions on the surface-structural rearrangements.

Angle-scanned XPD patterns were measured over a part of the hemisphere above the sample surface: Ba $4d$, Ti $2p$, and O $1s$ core-level photoelectron intensities were collected for polar emission angles from 11° to 69° and an azimuthal sector of more than 90°. The azimuthal angle was scanned in steps of 1°. For each value of the azimuthal angle, three fixed polar angles were measured. The analyzer has a polar acceptance of ~ 25° and the overall analyzer angular resolution is better than 0.2°. Using 700-eV photon energy, the kinetic energy for Ba $4d_{5/2}$ (610 eV), Ti $2p_{3/2}$ (240 eV), and O $1s$ (170 eV) gives inelastic mean-free-path values of 18.2, 9.5, and 6.9 Å, respectively.[22] The overall energy resolution (beamline and spectrometer) was 0.25 eV. All measurements were done at room temperature.

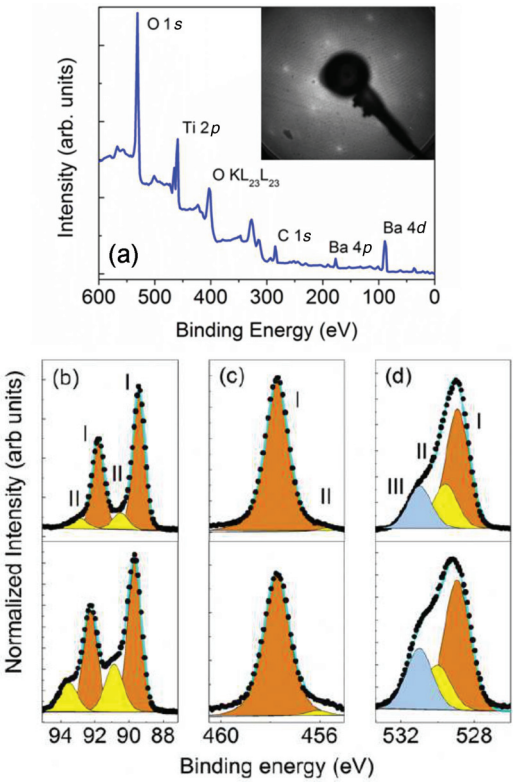

FIG. 3. (Color online) (a) Survey XPS scan of clean BTO(001) single crystal. Inset typical (1 × 1)LEED image of the BTO(001) surface. (b) Ba 4*d*; (c) Ti $2p_{3/2}$; (d) O 1*s* core-level spectra at normal (top) and 55° (bottom) surface-sensitive emission angles. The bulk perovskite emission (I) is dark gray (orange online), the surface-related components in the Ba 4*d* and O 1*s* spectra and the Ti^{3+} component in the Ti $2p_{3/2}$ spectrum are in gray (blue online) and light gray (yellow online).

B. Theory

The simulations of the XPD patterns were done in a multiple scattering approach using the multiple scattering for electron diffraction (MSCD) package,[23] implemented by a genetic algorithm suitable for exploring a large parameter space.[24] The number of elastic scattering events at low to moderate photoelectron kinetic energy makes it necessary to use multiple scattering calculations (MSC). In order to reduce computing time for the cluster calculations, we have followed a Rehrs-Albers (RA) approach in which the exact Green's function formalism is expressed in terms of scattering matrices expanded over all angular momentum quantum numbers *m* and *l*. The exact RA formalism is the curved-wave analogy to the plane-wave scattering. However, the scattering matrices can be safely truncated to second, third, or fourth order depending on the initial state of the electron. The higher-order versions of RA may be necessary for *d* and *f* initial states.[23] Since our photoelectron diffraction data include the Ba 4*d* emission, we use the fourth-order RA approximation and allow up to eight scattering events within the cluster. The structure was optimized using rumpling (relative cation/anion displacement) and interplanar relaxation parameters for the first atomic layers of both TiO_2-terminated and BaO-terminated BTO(001). The calculations were performed for a temperature of 300 K. The

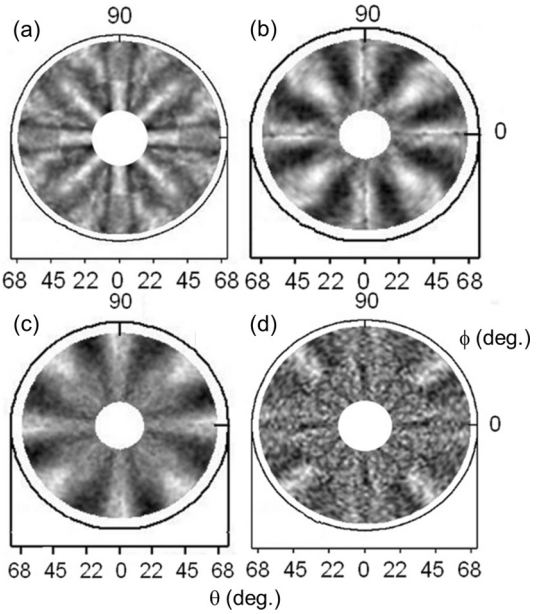

FIG. 4. Experimental XPD for BTO(001) obtained with 700-eV photon energy for (a) Ba 4*d*, (b) Ti 2*p*, (c) O 1*s*, and (d) C 1*s* emission. The XPD anisotropy, as defined by (Imax-Imin)/Imax, is 33%, 32%, 23%, and 8% for the Ba 4*d*, Ti 2*p*, O 1*s*, and C 1*s*, respectively.

radial matrix and atomic phase shifts were generated using a nonrelativistic self-consistent Hartree-Fock solution of the isolated atoms accompanied by the muffin-tin approximation. A parabolic cluster corresponding to the information depth of the XPD experiment is used with 12-Å radius and 25-Å depth, containing approximately 430 atoms. There are thus 85 unit cells in the final cluster, sufficient to simulate the XPD pattern. Additional emitters did not improve the results. The simulations are assessed with respect to the experimental data using a reliability factor *R*.[23] The smaller the *R* factor, the better the agreement with experiment. A perfect agreement corresponds to $R = 0$, no agreement is expressed by $R = 1$. For oxide structures with many parameters, a good *R* factor is typically lower than 0.30–0.40.[25]

III. RESULTS

A. XPS

Figure 3(a) shows a survey spectrum for the clean BTO(001) surface acquired using a photon energy of 700 eV. There is evidence for a small amount of surface C, 10 times weaker than the O 1*s* intensity after taking into account the relative cross sections. We have used the C 1*s* line (BE = 284.6 eV) to check the binding energy calibration. As shown in Fig. 4(d), the C 1*s* XPD signal has weak anisotropy, suggesting that the C shows weak local order. We assume that it does not systematically affect changes in the surface atomic positions.

The Ba $4d_{5/2}$, Ti $2p_{3/2}$, and O 1*s* core-level spectra taken at normal (top) and 55° angle (bottom) emission are shown in Figs. 3(b)–3(d). A Shirley background was subtracted from all the core-level spectra. The Ba 4*d* spectra have two components [see Fig. 3(d)]. The spectra were fitted using a mixed Gaussian/Lorentzian line shape (80%/20%) with a full width half maximum (FWHM) of 1.25 eV for both components

and a spin-orbit splitting of 2.55 eV. The binding energy (BE) of the main $4d_{5/2}$ component at normal (55°) emission is 89.64 (89.67) eV and the high binding-energy component (II) is at 90.76 (90.87) eV, thus the core-level shift is 1.13 (1.20) eV. At 55° off normal detection, peak II increases in intensity, suggesting it is due to emission from surface or near-surface atoms. This high binding-energy (HBE) component has been attributed to surface-layer Ba atoms with a lower oxygen coordination than in the bulk[26] although the core-level shifts found by Hudson *et al.* were slightly higher (1.3–1.4 eV for the Ba 4*d*). The shift is also similar to that observed on the clean surface of a thick $Ba_xSr_{1-x}TiO_3$ single-crystal film.[27] However, a HBE component is also observed on a clean, TiO_2-terminated surface of BTO where there are no surface Ba atoms.[25] The exact interpretation of the HBE component remains therefore an open question because the atomic rearrangement to screen the surface charge could also modify the electronic environment of the near-surface as well as surface Ba atoms.[25] The presence of different surface polarizations should, in principle, give rise to shifts in the measured core-level binding energies. As the XPD will show, the surface polarization is to a large extent screened by atomic reconstruction which probably attenuates the differences in the measured core-level binding energies. It would be possible to model the core-level spectra with three narrower peaks, shifted by the remnant polarization, however, this is beyond the scope of the present spectroscopic data. We have adopted the simplest possible deconvolution of the spectra with just two components.

The Ti $2p_{3/2}$ spectra in Fig. 3(c) are fitted with a FWHM of 1.3 eV and Gaussian/Lorentzian (80%/20%) line shapes. Both normal and grazing angle spectra have a main component (I) with a binding energy of 457.7 eV due to Ti bonding in the perovskite structure with valency of 4+. The component II, shifted by 1.8 eV to lower binding energy, is associated with Ti in a reduced (3+) valence state[28] due to the formation of oxygen vacancies after annealing.

In the O 1*s* spectrum taken at the normal emission [Fig. 3(d), top] there are three components: peak I at 529.10 eV (57.8% intensity) and peaks II and III at 529.58 eV (21.7%) and 530.94 eV (20.5%), respectively. Peak I is due to oxygen in the bulk perovskite environment, peak II, shifted by 0.7 eV, is associated with proton adsorption on surface lattice oxygen, and peak III to OH adsorption at on-top cation sites.[25] The spectrum taken at 55° emission also has three peaks. The intensity of peaks II and III increases, showing that they are indeed surface related.

To quantify the surface localization of the Ba HBE peak, we use a layer-by-layer attenuation model. Assuming a BaO-terminated surface, the fraction of the total Ba 4*d* intensity due to surface Ba atoms can be written as $(1 - k^2)$, where the layer attenuation factor k is given by $\exp[-c/2\lambda\cos(\theta)]$, λ is the inelastic mean-free path, θ the take-off angle, and c the lattice constant. Similarly, the fraction of the total O 1*s* intensity due to surface oxygen atoms is $(1 - k^2)/(2 + k)$. We assume that both BaO and TiO_2 have the same attenuation factor and use the inelastic mean-free-path values given above. The model predicts that a 0.20 (0.32) fraction of the total Ba 4*d* intensity is due to surface atoms at normal (55°) emission angle. For the O 1*s*, the predicted fraction is 0.18 (0.29). The respective experimental values for the Ba 4*d*, 0.14 (0.24), and for the O 1*s*, 0.23 (0.36), are close to the model predictions, suggesting that the surface is mainly BaO terminated. The difference between the measured and model values could be explained by an altered surface electronic environment extending over several atomic layers. The ionic displacements deduced from the XPD analysis discussed below provide further support for a changed near-surface environment. The fraction of Ti^{3+} increases from 1.6% to 3.5% of the total intensity when going from normal to 55° emission angle. Each oxygen vacancy V_O reduces two Ti^{4+} ions, and if we assume that V_O are created preferentially in the TiO_2 planes, then this corresponds to a near-surface V_O concentration of 0.9% (of the total number of surface oxygen atoms) in the first TiO_2 layer. Using the XPS intensities, tabulated sensitivity factors,[29] and inelastic mean-free paths,[30] we can estimate the bulk (surface) stoichiometry of the sample to be $Ba_{0.21}Ti_{0.20}O_{0.58}$ ($Ba_{1.1}TiO_{2.9}$), which is very close to the oxygen vacancy concentration as estimated from the Ti^{3+} intensity. The stoichiometry of the Ti does not change. The O desorption energy at the surface is lower than in the bulk, thus the reduction in oxygen content with annealing is correlated with an increase in the proportion of Ba at the surface.

B. XPD

1. Experimental XPD

In Figs. 4(a)–4(d), we present the experimental Ba 4*d*, Ti 2*p*, O 1*s*, and C 1*s* XPD patterns acquired using 700-eV photon energy. The data are presented in the form of a stereographic projection or diffractogram. Normal emission intensity is at the center and grazing angle emission is at the edge of the diffractogram. The XPD anisotropy, as defined by $(I_{max} - I_{min})/I_{max}$, is 33%, 32%, 23%, and 8% for the Ba 4*d*, Ti 2*p*, O 1*s*, and C 1*s*, respectively. The anisotropy is sharpest for the Ba 4*d* emission because the higher kinetic energy (KE) enhances forward focusing and thus the XPD signal reflects better the bulk crystal structure, assumed to be constant, rather than that of the surface which may vary over the first atomic layers. The angular anisotropy in the C 1*s* emission is low for most polar angles, only becoming significant at grazing emission, typical of disordered adsorbates, probably from residual gas in the chamber. The beam spot (~100 μm) on the sample is much larger than the typical domain width (~1 μm). The presence of domain ordering (visible to the eye) means that the XPD intensity anisotropies in the diffractograms correspond to a weighted sum of those due to the atomic structures of differently polarized domains. The aim of the simulations is to quantify the surface-structural changes in each domain and to estimate the proportion of each polarization present at the surface.

2. XPD simulations

There are four possible in-plane polarizations which can be labeled P_x, P_{-x}, P_y, and P_{-y}. From symmetry, each should have the same rumpling and relaxation in the z direction, i.e., perpendicular to the surface plane. From consideration of the elastic energy, there is no reason that there should be more of one particular in-plane polarization than another. We have assumed that all four in-plane polarizations are present in equal

proportions. The in-plane polarization P^{in} can then be written as $P^{in} = (P_x + P_{-x} + P_y + P_{-y})/4$. There are therefore three possible polarizations P^+, P^-, and P^{in}, satisfying the condition $N^+ + N^- + N^{in} = 1$, where N^+, N^-, and N^{in} are the fractions of each domain type contributing to the XPD signal. The surface atomic structure of each polarization over the first four atomic layers is described in terms of seven parameters: four layer rumpling values η_i and three interlayer relaxation parameters Δd_{ij}, giving in total 23 adjustable parameters. The R factor optimization of the Ba $4d$, Ti $2p$, and O $1s$ simulations must converge to the same result to give a reasonable solution. This is an extremely large parameter space and it is unrealistic to adjust all 23 parameters simultaneously and expect convergence to a global minimum. We have adopted the following three-step method, which we refer to as method (1).

In the first step, the R factor for each of the Ba $4d$, Ti $2p$, and O $1s$ XPD patterns is minimized with respect to the experimental diffraction pattern assuming a single polarization value. This is repeated for each of the three possible polarizations P^+, P^-, and P^{in}. The atomic positions are then fixed to these values and the R factors are optimized by a linear combination of P^+, P^-, and P^{in} for each XPD pattern. Since $N^+ + N^- + N^{in} = 1$, the R-factor results of the simulations can be presented in the form of a contour plots with N^+ and N^- axes. In the third step, to check self-consistency, N^+, N^-, and N^{in} are fixed at the average N^+, N^-, and N^{in} values for the three XPD patterns and all 21 structural parameters η_i and Δd_{ij} values are simultaneously relaxed.

We also tried a second method, method (2), which should, in principle, converge to the same solution. This consisted of first optimizing the linear combination of N^+, N^-, and N^{in} using the bulk rumpling and relaxation values. Then, the in-layer rumpling parameters and interlayer relaxation parameters are relaxed while keeping the linear combination fixed. The calculations using method (2) are presented in more detail in the Appendix. However, the simulations using bulk atomic positions as starting values to optimize the linear combination of N^+, N^-, and N^{in} do not converge. This is a further indication that the surface structure is significantly different from that of the bulk, too much, in fact, to allow convergence. In the following, all the XPD simulations have been carried out using method (1).

Prior to the first step, the nonstructural parameters were determined giving a 400-K Debye temperature and ~6 eV for the inner potential;[31] this calculation was performed for two possible terminations: BaO or TiO_2 surface. The Debye temperature represents an average value for the Ba, O, and Ti emitters. The experimental lattice positions of bulk tetragonal BTO were used as initial values.[29] For the in-plane polarization, the lateral positions were fixed at those given by Padilla and Vanderbilt.[10] The values of the nonstructural parameters were held constant in the final optimized structure.

The R-factor minimization as a function of rumpling and relaxation was done using a genetic algorithm for each (Ba $4d$, Ti $2p$, and O $1s$) XPD simulation.[24] The O $1s$ XPD pattern is used to ascertain the surface termination layer since the corresponding XPD data are the most surface sensitive. The experimental and simulated XPD azimuthal curves for BaO- or TiO_2-terminated surfaces at different polar angles (14.6°, 30.6°, 45.6°, and 68.6°), with a P^+ polarization are presented in Fig. 5. The better fit is systematically obtained for the BaO-terminated layer. All simulations were therefore done assuming that the surface is mainly BaO terminated. At 45.6° and 68.6°, there is asymmetry in the azimuthal anisotropy for which we do not have a simple explanation. The asymmetry is less obvious at 30.6°, closer to the sample normal, suggesting that it might be due to adsorbates to which the O $1s$ emission will be the most sensitive. The results for P^+, P^-, and P^{in} polarization states for the Ba $4d$, Ti $2p$, and O $1s$ after the first step of the R-factor optimization are shown in Fig. 6. The simulated Ba $4d$ patterns have the sharpest structure. This is to be expected since the higher kinetic energy will favor the forward scattering regime and is less sensitive to surface relaxations.

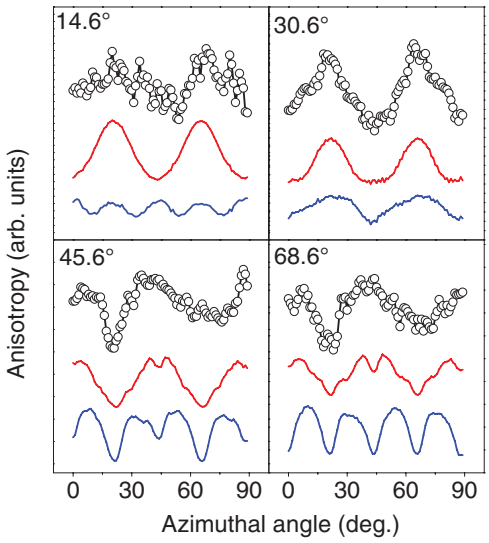

FIG. 5. (Color online) Experimental and simulated O $1s$ XPD azimuthal curves taken at polar angles of 14.6°, 30.6°, 45.6°, and 68.6°. The experimental anisotropy (circles) is compared with the simulations for TiO_2 [dark gray (blue)] and BaO [light gray (red)] terminations in P^+ polarization.

The results of the second step minimization of the R factor as a function of a linear combination of P^+, P^-, and P^{in} are reported in Fig. 7 in the form of R-factor contour plots for Ba $4d$ [Fig. 7(a)], Ti $2p$ [Fig. 7(b)], and O $1s$ [Fig. 7(c)]. The best N^+ and N^- values are read from the center of the minimum contour of the R factor. We note that the linear combination minimizing the R factor are close but not the same for all three XPD patterns. For the Ba $4d$, the R factor of a linear combination is minimized for a surface with approximately 56% P^+ and 44% P^- domains, for the Ti $2p$ XPD, the R factor is a minimum with 58% P^+, 8% P^- domains and 34% P^{in} and for the O $1s$ the minimum is found for 54% P^+ and 46% P^-. Figure 8 shows the average contour plot of the R factor as a function of polarization for the three XPD patterns. The minimum corresponds to 55% P^+, 38% P^-, and 7% P^{in}.

Finally, for each XPD pattern, Ba $4d$, Ti $2p$, and O $1s$, we have held the linear combination constant at 55% P^+, 38% P^-, and 7% P^{in} and iterated simultaneously the 21 rumpling and relaxation parameters. The atomic rumpling

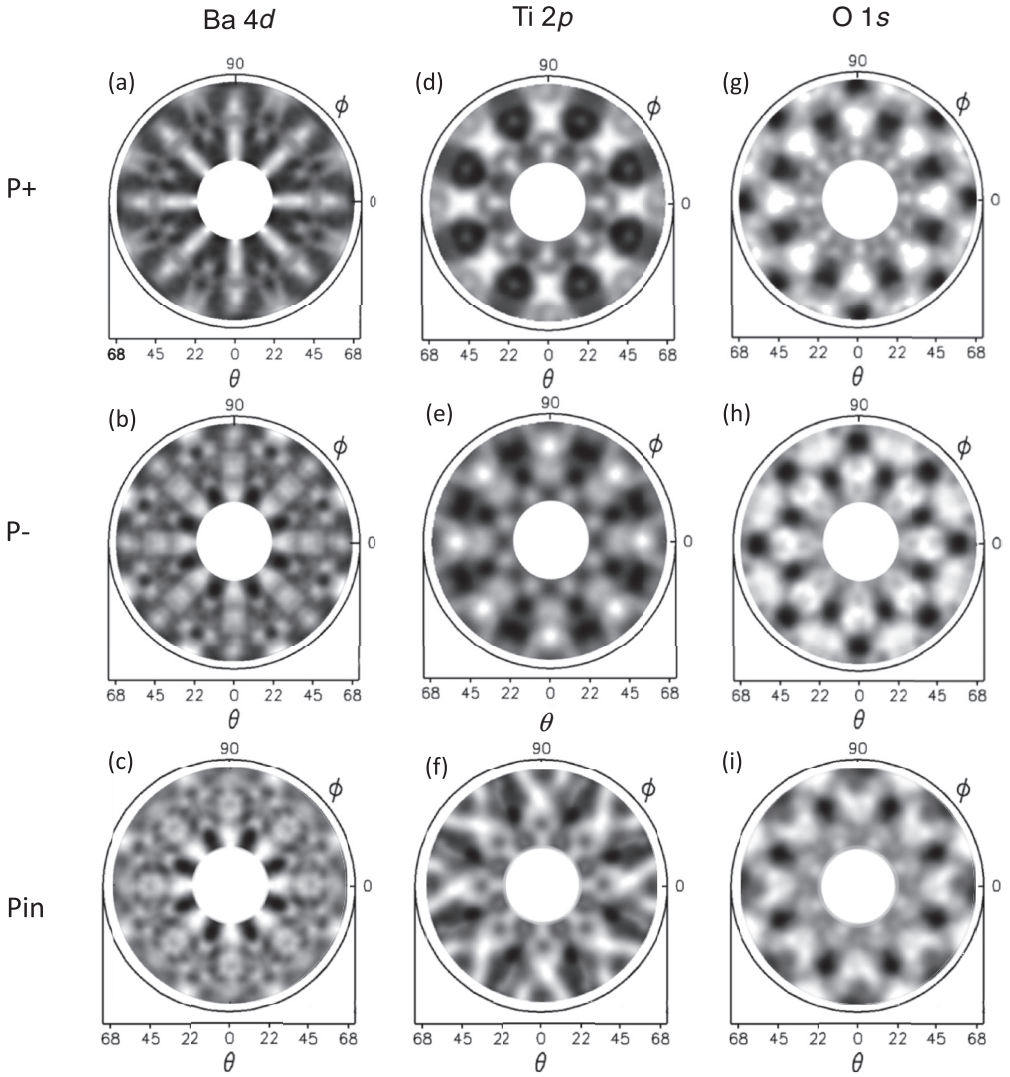

FIG. 6. Multiple scattering simulations of (a)–(c) Ba 4*d*, (d)–(f) Ti 2*p*, and (g)–(i) O 1*s* XPD for, from top to bottom, P^+, P^-, and P^{in} polarizations.

$\eta = [\delta_z(M) - \delta_z(O)]/2$ and the changes in the interplanar spacing Δd_{ij} are given in Tables I, II, and III for the Ba 4*d*, Ti 2*p*, and O 1*s* XPD simulations. Figure 9 compares the final simulated Ba 4*d* diffractogram obtained with the relaxed atomic positions for 55% P^+, 38% P^-, and 7% P^{in} domains with experiment. All of the experimental structure is reproduced. The simulated structure appears blurred in comparison with those of singly polarized domains in Fig. 6,

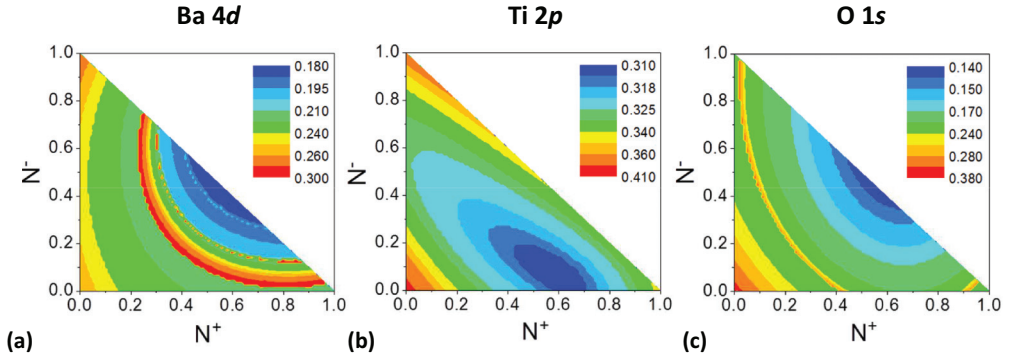

FIG. 7. (Color online) *R*-factor N^+/N^- contour plots for (a) Ba 4*d*, (b) Ti 2*p*, and (c) O 1*s* XPD simulations. N^+, N^-, and N^{in} are the proportions of P^+, P^-, and P^{in} domains contributing to the XPD signal satisfying the condition $N^+ + N^- + N^{in} = 1$ and it is assumed that $P^{in} = (P_x + P_{-x} + P_y + P_{-y})/4$.

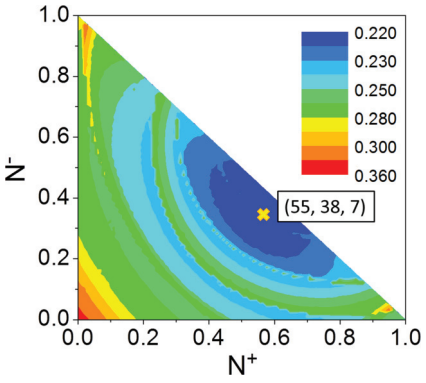

FIG. 8. (Color online) Average R-factor N^+/N^- contour plot of Fig. 7. The R-factor minimum is at 55% P^+, 38% P^-, and 7% P^{in}.

however, the much better R factor demonstrates that this blurring is in fact due to the simultaneous presence of different surface polarizations. It is therefore a real effect and not due to, for example, low statistics. The Ti $2p$ simulation shows similar agreement with experiment. The agreement is less good for the O $1s$, but this may be due to the residual surface contamination since the O $1s$ XPD is the most surface sensitive and should also show the strongest multiple scattering effects. Figures 10(a) and 10(b) are sectional schematics of the interplanar relaxation and intraplanar rumpling for the first four atomic layers in P^+ and P^- domains, respectively. The original and relaxed atomic layer positions are indicated by dotted and solid lines, respectively, obtained from the Ba $4d$ XPD pattern. The vertical atomic displacements have been multiplied by 10 for clarity.

Relaxing the atomic positions has considerably improved the agreement with experiment. The Ba $4d$ simulations using the bulk ferroelectric distortions gives an R factor of 0.50 whereas using the relaxed values the R factor is 0.18, underlined by the good agreement with experiment shown in Fig. 9.

IV. DISCUSSION

The rumpling and relaxation amplitudes in Fig. 10 vary when going from the surface layer into the bulk. The main atomic distortion in BTO is expected around the Ti ion, however, because of the longer inelastic mean-free path, the Ti $2p$ photoelectrons are more sensitive to the subsurface atomic layers than the O $1s$ and may give slightly less accurate values for surface-related atomic distortions. The Ba $4d$ XPD is the least sensitive to the surface structure and will therefore privilege the atomic distortion over all four atomic layers. On the other hand, the O $1s$ XPD is extremely surface sensitive with an inelastic mean-free path of 6.9 Å. The spread in depth sensitivities can actually be an advantage because the three XPD simulations are required to converge towards a common structure which describes changes in relaxation and rumpling going from the surface into the bulk.

The rumpling and interlayer relaxation in Tables I, II, and III can be compared with first-principles theory and experiment in the literature, reproduced in Table IV. A value of $c/2 = 2.018$ Å was used to obtain η and Δd_{ij}.[10,12,19]

The rumpling for $P^{\pm}$ states has the same sign as the polarization and is quantitatively similar for the three XPD patterns. The rumpling magnitude varies between 0.01 and 0.06 Å with a mean value of 0.028 Å (0.70% of the lattice parameter), whereas the magnitude of the interlayer relaxation varies between 0.01 and 0.13 Å with a mean value of 0.038 Å (0.95% of the lattice parameter) over the first four layers. In general, the rumpling increases deeper into the BTO, particularly for the Ba $4d$ results, whereas the Δd_{ij} values decrease towards the bulk. The Δd values obtained from the Ti $2p$ and O $1s$ simulations show a larger spread in values for the subsurface layers, possibly reflecting the higher surface sensitivity. Large rumpling and small interplanar relaxation

TABLE I. Atomic rumpling (η) and changes in interplanar spacing (Δd_{ij}) obtained from the final Ba $4d$ XPD simulations for out-of- and in-plane polarizations P^+, P^-, and P^{in}. All values are in Å.

	Ba $4d$		
	P^+	P^-	P^{in}
η_1	+0.02	−0.01	+0.02
η_2	+0.01	−0.03	+0.03
η_3	+0.04	−0.02	+0.01
η_4	+0.05	−0.05	+0.02
Δd_{12}	+0.14	+0.02	−0.02
Δd_{23}	−0.08	+0.03	+0.09
Δd_{34}	+0.01	−0.04	−0.06

TABLE II. Atomic rumpling (η) and changes in interplanar spacing (Δd_{ij}) obtained from the final Ti $2p$ XPD simulations for out-of- and in-plane polarizations P^+, P^-, and P^{in}. All values are in Å.

	Ti $2p$		
	P^+	P^-	P^{in}
η_1	+0.01	−0.01	+0.03
η_2	+0.02	−0.04	+0.03
η_3	+0.02	−0.02	+0.01
η_4	+0.05	−0.04	+0.02
Δd_{12}	−0.02	−0.02	−0.02
Δd_{23}	−0.04	+0.04	+0.05
Δd_{34}	+0.08	−0.03	−0.06

TABLE III. Atomic rumpling (η) and changes in interplanar spacing (Δd_{ij}) obtained from the final O $1s$ XPD simulations for out-of- and in-plane polarizations P^+, P^-, and P^{in}. All values are in Å.

	O $1s$		
	P^+	P^-	P^{in}
η_1	+0.01	−0.01	+0.03
η_2	+0.02	−0.04	+0.04
η_3	+0.03	−0.04	+0.01
η_4	+0.02	−0.06	+0.05
Δd_{12}	−0.02	−0.02	−0.04
Δd_{23}	−0.04	+0.04	+0.01
Δd_{34}	+0.05	0.00	−0.01

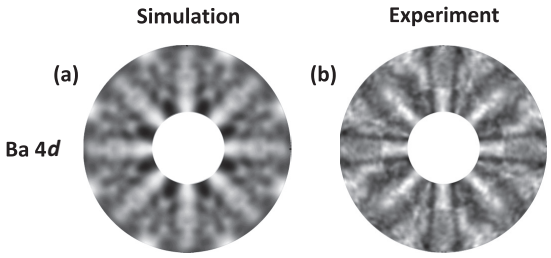

FIG. 9. (a) Final simulation of the Ba 4*d* diffractogram with relaxed atomic positions for 55% P^+, 38% P^-, and 7% P^{in} domains. (b) Experimental XPD data.

are consistent with bulk ferroelectric distortion, unaffected by surface boundary conditions. The lower rumpling at the surface is consistent with partial screening of surface polarization charge by atomic rearrangement, giving rise to a surface polarization lower than in the bulk. No significant change in rumpling or relaxation is observed beyond the fourth atomic layer, i.e., the FE distortion is no longer influenced by the surface and has adopted the bulk value. These results shed some new light on the nature of the surface "dead" layer. Atomic displacements can reduce the surface polarization but given the nonzero rumpling observed by XPD, the surface may not be completely dead in terms of ferroelectric polarization. This agrees with predictions made on the basis of first-principles calculations of a BaO-terminated in-plane polarized surface[32] and with a recent LEED I-V on an epitaxially strained BTO(001) thin film which showed that reconstruction can even give rise to a dipole inversion in the clean surface layer.[25] The persistence of rumpling at the surface implies a "remnant" surface ferroelectricity which to be stable must be screened, consistent with the presence of domain ordering. The interlayer

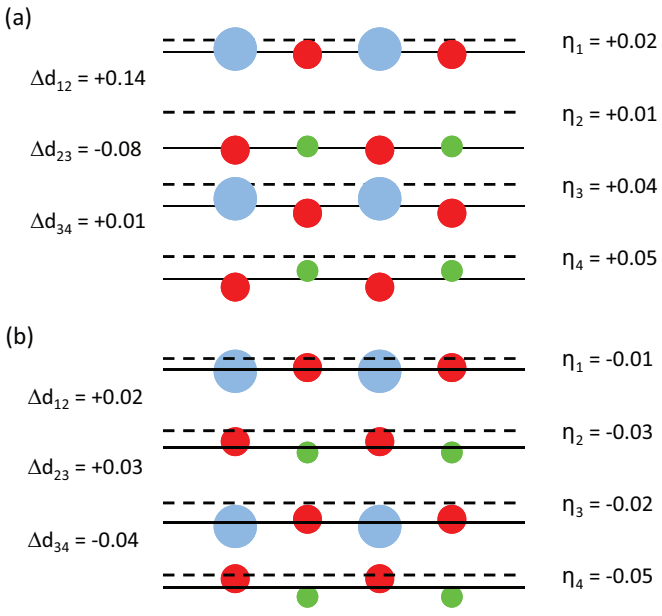

FIG. 10. (Color online) Relaxation and rumpling for the first four atomic layers in (a) P^+ and (b) P^- domains obtained from the Ba 4*d* XPD. The original and relaxed atomic layer positions are indicated by dotted and solid lines, respectively. The atomic displacements are multiplied by 10 for clarity. Color coding as in Fig. 1.

TABLE IV. Vertical atomic rumpling (η) and changes in interplanar spacing (Δd_{ij}) from first-principles calculations and experimental LEED data. The displacements of Ref. 16 were converted back to the absolute displacements using the calculated lattice parameter. The $\delta(O)$ value used in the TiO_2 plane is the average of the two oxygen displacements. All values are in Å.

	Literature		
	P^+ (Ref. 11)	P^{in} (Ref. 14)	P^- (Ref. 15)
η_1	+0.01	+0.03	−0.03
η_2	+0.03	+0.04	+0.04
η_3	+0.01	+0.03	+0.01
η_4	+0.03	+0.05	
Δd_{12}	−0.09	+0.02	−0.12
Δd_{23}	+0.16	−0.02	+0.04
Δd_{34}	−0.03	+0.02	

relaxation tends to zero going into the bulk, corresponding to a constant ferroelectric distortion, as expected far from the polarization discontinuity of the surface. These conclusions are in qualitative agreement with the results of Despont *et al.*[16] who found that the surface relaxation and rumpling also acted against the ferroelectric distortion in epitaxially strained $PbTiO_3$ films. The structural changes over the first two unit cells will modify the near-surface electronic environment; this aspect should be confirmed by more systematic experiments and calculations.

Not only does the XPD allow quantification of the local surface atomic distortions, it also points to the simultaneous presence of different surface polarizations. Similar information has also been obtained using photoelectron emission microscopy[33,34] (PEEM) and low-energy electron microscopy[25] (LEEM), however, the real-space imaging mode of these techniques does not allow direct probing of the microscopic atomic distortion. To do so would require LEEM imaging of the diffraction plane of the microscope in order to carry out a quantitative micro-LEED I-V experiment, giving similar information to that obtained by XPD, albeit without the chemical sensitivity of the latter. Although the parameter space is large, the full Ba 4*d*, Ti 2*p*, and O 1*s* XPD patterns constitute three independent measurements of the same atomic distortions, each of which is used to optimize the multiple scattering simulations. The *R*-factor minimization strategy has made use of a genetic algorithm and a step-by-step approach to a global minimum. The best solution is found for a linear combination of in- and out-of-plane surface domain polarizations. The good agreement with available literature values for the atomic rumpling and interplanar spacings and the consistency of three independent measurements of the ferroelectric distortions by the Ba 4*d*, Ti 2*p*, and O 1*s* XPD suggest that the method presented is fairly reliable. We therefore have a method which relates both to macroscopic FE domain ordering and microscopic surface reconstruction within each domain.

This interpretation does not attempt to quantify other forms of screening by adsorbates, defects, or free charge carriers. The Ti 2*p* XPS shows that there are V_O near the surface. We have assumed that the intrinsic contribution of V_O to polarization stability is the same for P^+ and P^-. However,

there is evidence that this may not be the case.[35] Further work is also needed in this direction. An obvious next step would be the use of spatially resolved XPD to distinguish a single FE domain. This could be done using a zone plate to obtain a microfocused beam smaller than the domain width. A fascinating experiment to carry out would be to measure the surface rumpling and relaxation as a function of the domain periodicity to determine more quantitatively the relative contributions of atomic reconstruction and domain ordering to the screening of the depolarizing field.

The V_O concentration is also an important question since it increases the sample conductivity. The formation of V_O by annealing in UHV was necessary in order to avoid charging under the synchrotron beam; too much conductivity would destroy the ferroelectric state. One recent study of BTO suggests that above a critical doping level of 1.36×10^{21} cm^3, a tetragonal to cubic, insulator-metal transition occurs.[36] This corresponds to a V_O concentration of 2%–3% with respect to the total oxygen content, higher than the values discussed here and estimated from the Ti^{3+} component of the Ti $2p$ spectra. The BTO surface studied here is therefore still ferroelectric despite the annealing treatment. An additional argument is that similar variations in the surface layer rumpling observed by Wang *et al.*[25] on a similar sample were inverted by dissociative adsorption of water. This would not be expected if, for example, the system had undergone a transition to a metallic, paraelectric state.

V. CONCLUSION

We have performed XPD using synchrotron radiation to determine the domain structure, atomic rumpling, and interplanar relaxation at the surface of BTO(001). After *ex situ* cleaning and *in situ* annealing in oxygen the surface is atomically flat with a preferential BaO termination plane and a (1×1) surface structure. Multiple scattering simulations of Ba $4d$, Ti $2p$, and O $1s$ XPD are performed using a genetic algorithm. Given the large parameter space, a three-step method is used to converge to a global R-factor minimum. Polarization-dependent rumpling and interplanar relaxation is determined and the proportion of in- and out-of-plane polarized domains obtained. At the surface of vacuum-annealed BTO(001) single crystal, the depolarizing field is screened by a combination of domain ordering and surface-structural changes. These results provide a complete experimental description of surface rumpling and relaxation as a function of polarization and a way of estimating the proportion of differently polarized surface domains. The large parameter space illustrates the complexity in probing the atomic structure in domain-ordered ferroelectric surfaces but also the potentially rich information available. The surface state is clearly an important issue in acquiring quantitative results and must be strictly controlled.

ACKNOWLEDGMENTS

A.P. was funded by CEA Eurotalents programme. This work was partially supported by the French National Research Agency (ANR) project Surf-FER, ANR-10-BLAN-1012, and by the CEA-IFA MUTLIFERRODMS project. We acknowledge SOLEIL for the provision of synchrotron radiation and Unicamp/IFGW/GFS group for the computational facilities. We thank M.-C. Asensio, J. Avila, I. Razado-Colambo of the ANTARES beam line for support and J. Leroy and B. Delomez for technical assistance.

APPENDIX: *R*-FACTOR MINIMIZATION METHOD (2)

The large parameter space (23 independent parameters consisting of the rumpling and relaxation parameters for each polarization and the proportions of P^+, P^-, and P^{in} domains) leads us to adopt an iterative method to find a reasonable minimum R factor between simulation and experiment. The method adopted is to minimize the atomic structure for each polarization state and the proportion of each polarization state separately before combining these results in a final optimization. These steps are done sequentially. Method (1), presented in the main body of the paper, optimized first the relaxation and rumpling values for each polarization, starting from the bulk ferroelectric distortion. The second step was then to optimize the values of N^+, N^-, and N^{in}, the proportions of each ferroelectric domain type. Here, we present the results of method (2). First, the linear combination of N^+, N^-, and N^{in} is found using the bulk atomic structure in the ferroelectric phase. Then, with N^+, N^-, and N^{in} fixed, the rumpling and relaxation for each polarization has been optimized. The results are shown in Figs. 11(a)–11(c). Three very distinct minima are found for the Ba $4d$, Ti $2p$, and O $1s$ XPD simulations. The minima are also much shallower than those obtained using method (1), illustrated in Fig. 7. It was not possible to find a global minimum using this second method. Furthermore, the R factors obtained are much larger than those of method (1). We interpret this as being due to the use of the bulk ferroelectric distortion without relaxation and rumpling as starting values for the simulations to search for the best linear combination of N^+, N^-, and N^{in}. Such values are too far from those

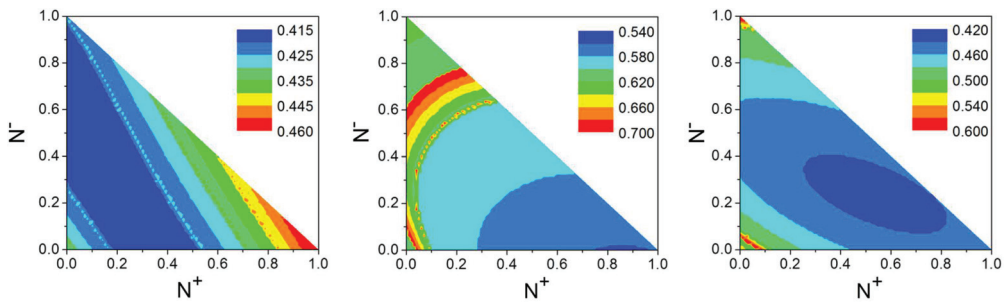

FIG. 11. (Color online) R-factor N^+/N^- contour plots for (a) Ba $4d$, (b) Ti $2p$, and (c) O $1s$ XPD simulations.

giving a consistent solution with method (1), even for the genetic algorithm. In other words, there are indeed significant structural changes in the first few atomic layers of BTO(001) with respect to the bulk FE structure.

*Correspondence should be addressed to nick.barrett@cea.fr

[1] J. Goniakowski, F. Finocchi, and C. Noguera, Rep. Prog. Phys. **71**, 016501 (2008).

[2] J. E. Spanier, A. M. Kolpak, J. J. Urban, I. Grinberg, L. Ouyang, W. S. Yun, A. M. Rappe, and H. Park, Nano Lett. **6**, 735 (2006).

[3] I. Krug, N. Barrett, A. Petraru, A. Locatelli, T. O. Mentes, M. A. Niño, K. Rahmanizadeh, G. Bihlmayer, and C. M. Schneider, Appl. Phys. Lett. **97**, 222903 (2010).

[4] C. L. Jia and K. Urban, Science **303**, 2001 (2004).

[5] W. J. Merz, Phys. Rev. **95**, 690 (1954).

[6] T. Shimada, S. Tomoda, and T. Kitamura, Phys. Rev. B **81**, 144116 (2010).

[7] M.-Q. Cai, Y.-J. Zhang, Z. Yin, and M.-S. Zhang, Phys. Rev. B **72**, 075406 (2005).

[8] A. M. Kolpak, D. Li, R. Shao, A. M. Rappe, and D. A. Bonnell, Phys. Rev. Lett. **101**, 036102 (2008).

[9] P. Forsbergh Jr., Phys. Rev. **76**, 1187 (1949).

[10] J. Padilla and D. Vanderbilt, Phys. Rev. B **56**, 1625 (1997).

[11] M. Fechner, S. Ostanin, and I. Mertig, Phys. Rev. B **77**, 094112 (2008).

[12] B. Meyer and D. Vanderbilt, Phys. Rev. B **63**, 205426 (2001).

[13] J. Osterwalder, T. Greber, A. Stuck, and L. Schlapbach, Phys. Rev. B **44**, 13764 (1991).

[14] B. Schneider, R. Niemann, C. Kuper, H. Hesse, and M. Neumann, J. Electron Spectrosc. Relat. Phenom. **96**, 37 (1998).

[15] A. Berlich, H. Strauss, C. Langheinrich, A. Chassé, and H. Morgner, Surf. Sci. **605**, 158 (2011).

[16] L. Despont, C. Koitzsch, F. Clerc, M. G. Garnier, P. Aebi, C. Lichtensteiger, J.-M. Triscone, F. J. Garcia de Abajo, E. Bousquet, and P. Ghosez, Phys. Rev. B **73**, 094110 (2006).

[17] L. Despont, C. Lichtensteiger, F. Clerc, M. G. Garnier, F. Garcia de Abajo, M. a. Van Hove, J.-M. Triscone, and P. Aebi, Eur. Phys. J. B **49**, 141 (2006).

[18] A. Winkelmann, C. S. Fadley, and F. J. Garcia de Abajo, New J. Phys. **10**, 113002 (2008).

[19] J. Shin, V. B. Nascimento, A. Y. Borisevich, E. W. Plummer, S. V. Kalinin, and A. P. Baddorf, Phys. Rev. B **77**, 245437 (2008).

[20] A. Hirata, A. Ando, K. Saiki, and A. Koma, Surf. Sci. **310**, 89 (1994).

[21] M. Kuwabara, H. Matsuda, N. Kurata, and E. Matsuyama, J. Am. Ceram. Soc. **80**, 2590 (1997).

[22] S. Tanuma, C. J. Powell, and D. R. Penn, Surf. Interface Anal. **21**, 165 (1994).

[23] Y. Chen, F. J. García de Abajo, A. Chassé, R. X. Ynzunza, A. P. Kaduwela, M. A. Van Hove, and C. S. Fadley, Phys. Rev. B **58**, 13121 (1998).

[24] M. L. Viana, R. Díez Muiño, E. A. Soares, M. A. Van Hove, and V. E. de Carvalho, J. Phys.: Condens. Matter **19**, 446002 (2007).

[25] J. L. Wang, F. Gaillard, A. Pancotti, B. Gautier, G. Niu, B. Vilquin, V. Pillard, G. L. M. P. Rodrigues, and N. Barrett, J. Phys. Chem. C **116**, 21802 (2012).

[26] L. T. Hudson, R. L. Kurtz, S. W. Robey, D. Temple, and S. R. L., Phys. Rev. B **47**, 10832 (1993).

[27] J. D. Baniecki, M. Ishii, T. Shioga, K. Kurihara, and S. Miyahara, Appl. Phys. Lett. **89**, 162908 (2006).

[28] J. L. Wang, B. Vilquin, and N. Barrett, Appl. Phys. Lett. **101**, 092902 (2012).

[29] T. Mitsui, E. Nakamura, and K. Gesi, *Numerical Data and Functional Relationships in Science and Technology*, edited by K.-H. Hellwege and A. Hellwege (Springer, Berlin, 1981).

[30] C. Wagner, W. Riggs, L. Davis, and J. Moulder, *Handbook of X-Ray Photoelectron Spectroscopy*, edited by G. Muilenberg (Perkin-Elmer Corporation, Eden Prairie, 1979).

[31] V. B. Nascimento, R. G. Moore, J. Rundgren, J. Zhang, L. Cai, R. Jin, D. G. Mandrus, and E. W. Plummer, Phys. Rev. B **75**, 035408 (2007).

[32] G. Geneste and B. Dkhil, Phys. Rev. B **79**, 235420 (2009).

[33] A. Höfer, M. Fechner, K. Duncker, M. Hölzer, I. Mertig, and W. Widdra, Phys. Rev. Lett. **108**, 087602 (2012).

[34] J. E. Rault, W. Ren, S. Prosandeev, S. Lisenkov, D. Sando, S. Fusil, M. Bibes, A. Barthélémy, L. Bellaiche, and N. Barrett, Phys. Rev. Lett. **109**, 267601 (2012).

[35] Y. Mi, G. Geneste, J. E. Rault, C. Mathieu, A. Pancotti, and N. Barrett, J. Phys.: Condens. Matter **24**, 275901 (2012).

[36] Y. Iwazaki, T. Suzuki, Y. Mizuno, and S. Tsuneyuki, Phys. Rev. B **86**, 214103 (2012).